International Journal of Energy and Environmental Engineering
a SpringerOpen Journal

ORIGINAL RESEARCH Open Access

Wind tunnel testing and numerical simulation on aerodynamic performance of a three-bladed Savonius wind turbine

Khandakar Niaz Morshed[1], Mosfequr Rahman[2*], Gustavo Molina[2] and Mahbub Ahmed[3]

Abstract

The purpose of this research work is to investigate experimentally and computationally the feasibility of improving the performance of the vertical-axis Savonius wind turbine. The authors first performed a series of wind tunnel investigations on semi-cylindrical three-bladed Savonius rotor scale models with different overlap ratios and without overlap. These experiments were conducted in front of a low-speed subsonic wind tunnel at different Reynolds numbers. Pressures around the concave and convex surfaces of each blade, as well as the static torque for the rotor models, were measured. Using these experimental data, the authors calculated aerodynamic characteristics such as drag coefficients, static torque coefficients, and power coefficients. The authors then performed computational fluid dynamics (CFD) simulations using the commercial CFD software FLUENT and GAMBIT to analyze the static rotor aerodynamics of those models. The experimental and computational results were then compared for verification. Three different models with different overlap ratios were designed and fabricated for the current study to find the effect of overlap ratios. The results from the experimental part of the research show a significant effect of overlap ratio and Reynolds number on the improvement of aerodynamic performance of the Savonius wind turbine. At higher Reynolds number, the turbine model without overlap ratio gives better aerodynamic coefficients, and at lower Reynolds number, the model with moderate overlap ratio gives better results.

Keywords: Savonius wind turbine, Aerodynamic performance, Torque coefficient, Power coefficient, Angle of rotation, Overlap ratio

Background

Background of Savonius wind turbine

Vertical-axis wind turbines (VAWTs) include both a drag-type configuration, such as the Savonius rotor, and a lift-type configuration, such as the Darrieus rotor. The simplest type of vertical-axis wind turbine is the Savonius rotor, the operation of which depends on the difference in drag force when the wind strikes either the convex or concave part of its semi-cylindrical blades. Savonius rotors are good at self-starting and work independently of wind direction. However, its efficiency is relatively lower than that of the lift-type VAWTs. Due to its simple design and low construction cost, Savonius rotors are primarily used to pump water and generate wind power on a small scale, and its large starting torque makes it suitable for starting other types of wind turbines that have inferior starting characteristics, such as the Darrieus rotor and Gyro mill [1]. Recently, some generators with high torque at low rotational speed, suitable for small-scale wind turbines, have been developed, suggesting that Savonius rotors may yet be used to generate electric power [1].

Wind turbine aerodynamics must be designed for optimal output to exploit the wind energy in a specific location. Diaz et al. [2] analyzed the drag and lift coefficients of a Savonius wind turbine to quantify the aerodynamic performance of the rotor. They found that maximum efficiency, in terms of power coefficient, occurs at a tip speed ratio of $\lambda = 1$, and the drag coefficient decreases sharply when the tip speed ratio increases or decreases

* Correspondence: mrahman@georgiasouthern.edu
[2]Mechanical Engineering Department, Georgia Southern University, Statesboro, GA 30460, USA
Full list of author information is available at the end of the article

from this value. They also found that the most important region of Savonius rotor operation occurs at a tip speed ratio around $\lambda = 1$, where the lift coefficient remains as a constant 0.5. Sawada et al. [3] studied the mechanism of rotation of a Savonius rotor with two semi-cylindrical blades and found that a rotor with a gap ratio of 0.21 produces positive static torque at all angles. They also found that lift force contributes significantly to dynamic torque, while the rotor angle is between $\alpha = 240°$ and $\alpha = 330°$. Aldoss and Obeidat [4] used the discrete vortex method to analyze the performance of two Savonius rotors running side-by-side at different separations. They compared their computational results on torque and power coefficients with their experimental results for verification. Fujisawa and Gotoh [5] studied the aerodynamic performance of a Savonius rotor by measuring pressure distribution on the blade surfaces at various rotor angles and tip speed ratios. Torque and power performance, evaluated by integrating the pressure, were in close agreement with direct torque measurements.

Rahman et al. [6-8] experimentally studied aerodynamic characteristics, such as the torque and drag coefficients, of a three-bladed Savonius rotor model by measuring the pressure difference between the convex and concave surfaces of each semi-cylindrical blade of the stationary rotor at different rotor angles and the variation of the separation point with the increase of rotor angle. They used the static coefficients for dynamic prediction and compared the findings in terms of power coefficients for different tip speed ratios with experimental results for the two-bladed Savonius rotor. Rahman et al. [9] conducted both experimental investigations and computational fluid dynamic (CFD) simulations to establish the feasibility of improving the performance of a simple, three-bladed Savonius VAWT. The normal drag coefficient, tangential drag coefficient, and torque coefficient were calculated both experimentally and numerically, and the results were compared. In each case, the calculations matched well. The numerical results were more accurate and gave positive values for combined drag coefficients and the total static torque coefficient.

Gupta et al. [10] compared a three-bucket Savonius wind turbine with a three-bucket Savonius-Darrieus wind turbine. They found that the power coefficient of the combined turbine decreases as the overlap ratio increases. The maximum power coefficient of 51% was found where there was no overlap. They claimed that the combined rotor without overlap, which showed 51% efficiency, was the highest efficiency of a Savonius wind turbine at any overlap condition under these test conditions. Altan et al. [11] did some experimental studies to improve the performance of the Savonius wind turbine using a curtain. They placed the curtain arrangement in front of the rotor in a configuration capable of preventing the negative torque that affects the convex blade surface of the Savonius wind turbine.

Sargolzaei and Kianifar [12] simulated a Savonius wind turbine using artificial neural networks (ANNs) to estimate power ratio and torque. They experimentally investigated seven prototype Savonius wind turbines and compared the experimental results with their predicted ANN results. Their predicted results were in good agreement with their experimental results. They found that increased wind speed causes torque increase. For all their models, they found that maximum torque was at 60° and minimum torque was at 120°. Altan and Atilgan [13] numerically simulated their experimental work using FLUENT 6.0 and GAMBIT 2.0. Their model was two-dimensional, and they used a standard k-ε turbulence model. To calculate pressure and velocity distribution, they used a semi-implicit method for pressure-linked equation (SIMPLE) analysis algorithm. By comparing the numerical and experimental results, they concluded that the curtain improved the performance of Savonius wind turbines.

Saha et al. [14] fabricated a two-stage Savonius wind turbine by inserting valves on the concave side of the blades. They compared its performance to a conventional Savonius wind turbine and found that with valves on a three-bladed turbine, the power coefficient was higher compared to a two-bladed turbine for both semi-circular and twisted blades. Without valves, air strikes the blades and rotates them in a negative direction. Saha et al. also varied the number of stages in a Savonius wind turbine and found that while the power coefficient increased from one to two stages, it decreased from two to three stages due to increased inertia. They tested the twisted blades of one, two, and three stages and found that the three stages had a better power coefficient, and the twisted blades showed better performance.

To decrease the variation in static torque in conventional Savonius rotors at a 0° to 360° rotor angle, Kamoji and Kedare [15] tested a helical rotor with a twist of 90°. They conducted experiments in an open-jet wind tunnel at gap ratios of 0.0, 0.05, and 0.08 to study the effect of gap ratio and Reynolds number on its performance and evaluated static torque, dynamic torque, and power coefficients. They compared its performance with and without a shaft between the end plates at different gap ratios. A helical rotor without a shaft was also compared with the performance of the conventional Savonius rotor. They found that all helical rotors have a positive coefficient of static torque at all rotor angles, but the rotors with a shaft had a lower power coefficient than those without. The coefficient of power of the rotor without a shaft with a 0.0 gap ratio was marginally less than the conventional Savonius rotor.

Gupta et al. [16] investigated the performance of two-bladed Savonius turbine with five overlaps of 16.2%, 20%, 25%, 30%, and 35%. Among them, 16.2% overlap condition showed maximum power extraction. The pressure drop across the rotor from upstream to downstream as well as the maximum pressure difference across the returning bucket is displayed in the same condition. Qasim et al. [17] worked with impeller scoop-frame type with movable vanes wind turbine (VAWT). The objective was to maximize the drag factor by closing the vanes on convex shape and opening when air hits the concave part. Due to the movement of vanes for and against the wind, a higher drag factor is worked on the impeller scoop-frame type with movable vanes and has higher efficiency than flat vanes.

Ghatage and Jyeshtharaj [18] have done an experiment by changing the shape of the blade as well as the blade number. They have studied with both regular curved blade and twisted curved blade. The experiment concluded that the two blades with twist enhance the efficiency of turbine. In their experiment, the 30°-twisted two-bladed turbine gave the better power coefficient. It can be concluded that the twisted blade attributes relatively higher drag over the turbine surface.

Kumbernuss et al. [19] studied two-staged Savonius-type turbines with different number of blades, the shape of the blades, the overlap ratio, and the phase shift angle. The wind turbine was tested under four different wind speeds of 4, 6, 8, and 10 m/s. There were three turbines with the overlap ratios of 0, 0.16, and 0.32. The overlap ratio of 0.16 produced the better performance among the three, followed by the 0.32 overlap ratio. At lower and higher air velocities, the larger and smaller phase shift angles, respectively, will produce better performance of the turbines.

Carrigan et al. [20] had the objective to introduce and demonstrate a fully automated process for optimizing the airfoil cross section of a vertical-axis wind turbine. The objective was to maximize the torque while enforcing typical wind turbine design constraints such as tip-speed ratio, solidity, and blade profile. This work successfully demonstrated a fully automated process for optimizing the airfoil cross section of a VAWT.

Researchers from different parts of the world have been investigating the aerodynamic characteristics of Savonius wind turbines and trying to identify the optimum design in order to achieve better performance compared to horizontal-axis wind turbines. Although much research has been going on experimentally and numerically on Savonius wind turbine performance improvement, there are few to no comprehensive studies using both experimental and numerical methods for various gap ratios at different Reynolds numbers. The primary goal of the present study is to investigate the aerodynamic characteristics of three-bladed Savonius wind turbines in order to contribute to the performance improvement of vertical-axis Savonius wind turbines. To achieve this goal, the authors designed and fabricated Savonius wind turbine scale models with no overlap ratio and two different overlap ratios, measured the pressure distribution around the Savonius turbine rotor models, and calculated the drag coefficients. Static torque was measured using the subsonic wind turbine for all models at varying angles of rotation, the mesh was generated numerically around all turbine models using GAMBIT, and fluid flow fields around the models were solved using k-ε turbulence model of FLUENT. Pressure contours, velocity contours, and torque were determined at various Reynolds numbers. A detail of the experimental and computational procedure of this research work can be found in the thesis work done by one of the authors [21].

Methods

Experimental measurement

Subsonic wind tunnel

A subsonic wind tunnel was designed and built to conduct the experimental measurement of this research as shown in Figure 1. The wind tunnel is 12-ft (3.66 m) long and consists of a converging mouth entry, honeycomb Section Background, test section, fan section, rectangle section, honeycomb Section Methods, converging diverging section, and rectangular exit section.

Mathematical expressions

The following equations were used to calculate various experimental aerodynamic coefficients corresponding to different Reynolds numbers (Re) and tip speed ratios (λ). Savonius rotor model dimensions and wind tunnel measured data were used as inputs for these equations.

Figure 1 Subsonic wind tunnel.

Rotor area:

$$A = DH. \tag{1}$$

Overlap ratio:

$$\mathrm{OR} = \frac{a}{D}. \tag{2}$$

Aspect ratio:

$$\mathrm{AR} = \frac{H}{d}. \tag{3}$$

Angular velocity:

$$\omega = \frac{2\pi N}{60}. \tag{4}$$

Reynolds number:

$$Re = \frac{VD}{\nu}. \tag{5}$$

Tip speed ratio:

$$\lambda = \frac{\omega D}{2V} \tag{6}$$

Torque coefficient:

$$C_{\mathrm{q}} = \frac{T}{\frac{1}{4}\rho A D V^2}. \tag{7}$$

Power coefficient:

$$C_{\mathrm{p}} = \frac{P}{\frac{1}{2}\rho A V^3} = \frac{T\omega}{\frac{1}{2}\rho A V^3} = C_{\mathrm{q}} \times \lambda. \tag{8}$$

Normal drag force:

$$F_{\mathrm{n}} = \int_0^{\pi} \Delta p \frac{d}{2} \cos\varnothing d\varnothing = \sum_{i=1}^{17} \Delta p_i \frac{d}{2} \cos\varnothing_i \Delta\varnothing_i. \tag{9}$$

Tangential drag force:

$$F_{\mathrm{t}} = \int_0^{\pi} \Delta p \frac{d}{2} sin\varnothing d\varnothing = \sum_{i=1}^{17} \Delta p_i \frac{d}{2} \sin\varnothing_i \Delta\varnothing_i. \tag{10}$$

Normal drag coefficient:

$$C_{\mathrm{n}} = \frac{F_{\mathrm{n}}}{\frac{1}{2}\rho V^2 A}. \tag{11}$$

Tangential drag coefficient:

$$C_{\mathrm{t}} = \frac{F_{\mathrm{t}}}{\frac{1}{2}\rho V^2 A}. \tag{12}$$

Drag force measurement

The pressure distribution around the concave and convex surfaces of each blade was measured experimentally using a semi-cylindrical three-bladed Savonius VAWT model with overlap distance, $a = 25$ mm, between the adjacent blades as shown in Figure 2. The rotor model was made of stainless steel with each blade diameter, $d = 125$ mm, height, $H = 300$ mm, and rotor diameter, $D = 225$ mm. The overlap ratio (OR) was 0.11, and no shaft was used through the rotor model. The whole rotor was mounted on an iron frame using two separate shafts and bearings at the two ends. The convex and concave surface pressures of each blade were measured at 17 tapping points using 1.5-mm outer diameter and 10-mm-long copper tubes which were press fitted into 17 tapping holes. Those tapping points were located at the mid-plane of each blade to measure the pressure at every 10° interval on the blade surface. The copper tubes were connected to 17 pressure transducers (PX277, Omega Engineering Inc., Stamford, CT, USA) through the 2-mm PVC tubes. Pressures were measured statically at every 30° interval of

Figure 2 Setup of Savonius rotor model with pressure transducer data acquisition system for drag force measurement.

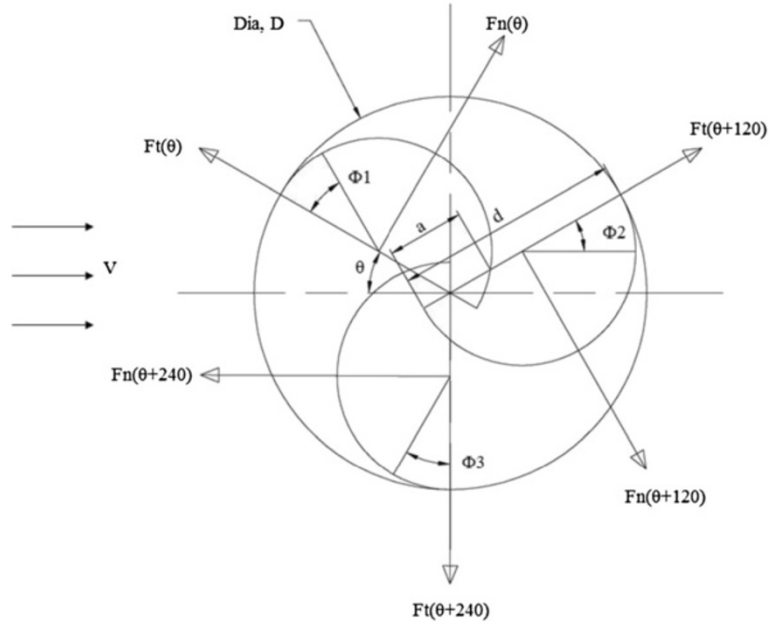

Figure 3 Schematic of the rotor model cross section. Showing the normal and tangential drag forces on each blade.

rotor angle. A personal computer equipped with a data acquisition system was used to record and edit the pressure data. Average wind speed during this experiment was 9.61 m/s. The Reynolds number based on rotor diameter was 1.47×10^5. The normal and tangential drag forces on each blade of the Savonius rotor model were calculated using the measured pressure difference between the concave and convex surfaces of the blades using Equations 9 and 10. Figure 3 shows the cross section of the rotor with the normal and tangential drag force directions. Tangential and normal drag coefficients were then calculated using Equations 11 and 12.

Three-bladed Savonius rotor models

To observe the effect of the OR (the ratio between the distance of the two adjacent blades and the rotor diameter) and Reynolds number on the aerodynamic characteristics of the Savonius rotor, three different rotor models with and without overlap ratios were designed and physically fabricated. Figure 4 shows the three Savonius rotor models with three different ORs. Model 1 was designed without any overlap between the adjacent blades and fabricated with three semi-cylindrical blades of diameter, $d = 127$ mm, and height, $H = 300$ mm. The blades of model 1 were made of acrylic and set 120° apart. The overall diameter of the rotor model 1 was $D = 248$ mm without any central shaft. Model 2 was designed with an overlap distance between the adjacent blades, $a = 25$ mm but having the same blade diameter and height as model 1, and was fabricated with the same number of blades 120° apart. The overall rotor diameter of model 2 was $D = 216$ mm with OR = 0.12. Model 3 was designed and fabricated with an overlap distance between adjacent blades, $a = 50$ mm,

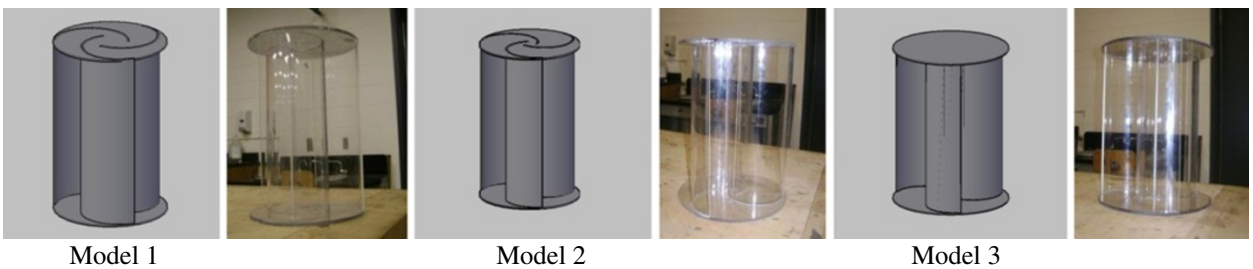

Figure 4 3-D and fabricated views of three Savonius rotor models.

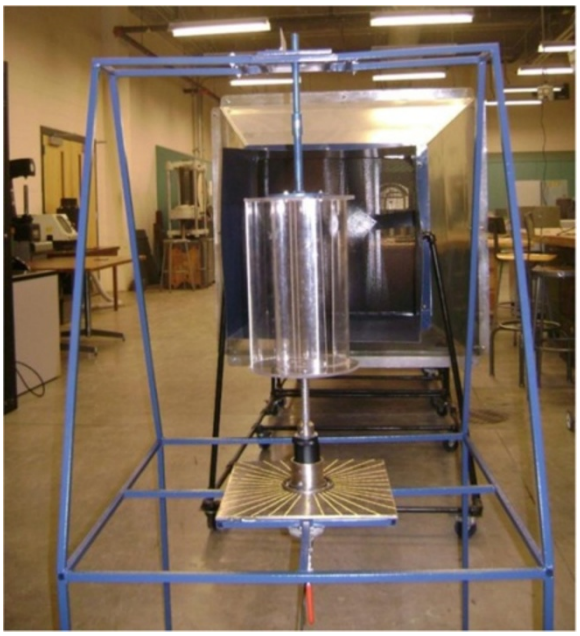

Figure 5 Setup of wind tunnel and Savonius rotor model for static torque measurement.

with the same blade diameter, height, and number of blades set 120° apart as model 1 and model 2. The overall rotor diameter of model 3 was $D = 192$ mm and OR = 0.26. These three models were tested in front of the subsonic wind tunnel for various Reynolds number flow conditions.

Static torque measurement

The experiment was carried out at three different wind speeds: $V = 9.66$, 8.23, and 7.33 m/s. The Reynolds numbers based on the rotor diameter varied from 9.94×10^4 to 1.6×10^5. Experiments were carried out, and data were recorded at room temperature. Static torque (T) for the three different models of the Savonius wind turbine was measured using a static torque meter (TQ-8800 model, Lutron Electronic Enterprise Co., Ltd., Taipei, Taiwan) at three different wind speeds. Torque meter output was in pound-inch which was then converted into Newton-meter. Rotational speed (N) was measured using a non-contact photo tachometer. Equation 4 was used to calculate the angular velocity from the rotational speed.

Savonius wind turbine is a drag-type VAWT where the lift forces are considered to be negligible. Figure 5 shows the experimental setup for torque measurement of a Savonius wind turbine model. When the wind strikes the blade surfaces of the model, two components of drag force are generated on each blade surface. Normal drag force (F_n) acts perpendicularly on the blade surface, and the tangential drag force (F_t) acts tangentially on each blade, as shown in Figure 3. The pressure difference between the concave and convex surfaces on each blade produces these tangential and normal drag forces. These components of drag force are responsible for torque generation within the turbine shaft and can be measured using a torque meter. Equation 7 is used to calculate the torque coefficient from the measured torque value. The power coefficient can be calculated from the measured torque and angular velocity of the rotor using Equation 8.

Numerical investigation

Numerical model selection

For the selection of the numerical model from the CFD code FLUENT 2D, a NACA 4412 airfoil was numerically

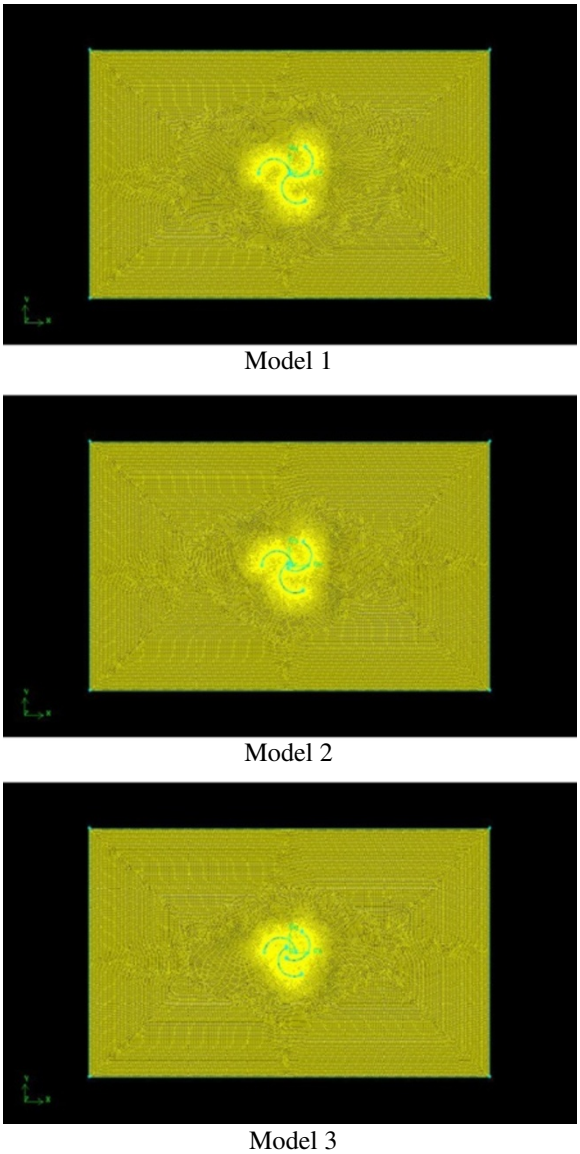

Figure 6 Generated mesh using GAMBIT.

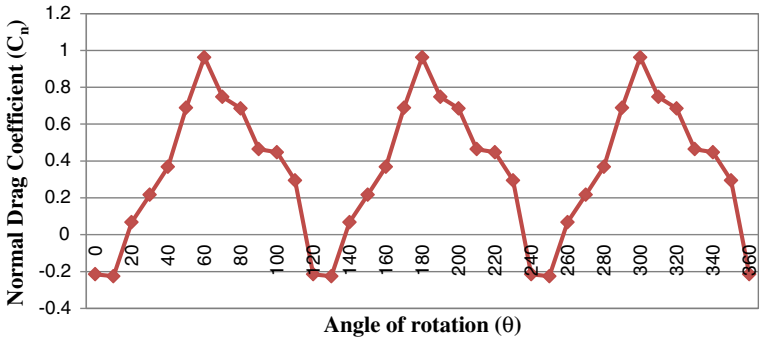

Figure 7 C_n **versus angle of rotation (*θ*) for a three-blade combined effect.**

examined at a different angle of attack and compared with established research results. Using the flow simulation results from both the inviscid model and the *k-ε* turbulence model, lift coefficient was calculated and then compared with published [22] NACA 4412 airfoil results. Comparing the inviscid model and the *k-ε* turbulence model results with established published results, it was found that the *k-ε* turbulence model gave more accurate results than the inviscid model. Therefore, the *k-ε* turbulence model was selected for numerical modeling of the Savonius wind turbine.

Numerical procedure

The *k-ε* turbulence model was used for the computational flow simulation around the Savonius rotor models with different overlap ratios. Commercially available software FLUENT was used to solve the turbulent flow field, and GAMBIT was used for mesh generation around the rotor models. Numerical simulation provides the pressure and velocity values at all nodal points of flow domain around the rotating blades. Figure 6 shows the 2-D mesh generated using GAMBIT within a computational domain around three-bladed Savonius wind turbine models in which the position of the three blades were 0°, 120°, and 240°. The size of the computational domain was 1.6 m × 1.4 m, and the total number of nodes was around 39,992. These computer-generated meshes were then exported into FLUENT for post-processing. The flow of air within the domain around the rotor model was assumed to be turbulent, and the effects of molecular viscosity were considered negligible. Also, the end effects of the turbine have been considered negligible. The simplest 'complete models' of turbulence are two-equation models in which the solution of two separate transport equations allows the turbulent velocity and length scales to be independently determined.

The standard *k-ε* turbulence model in FLUENT was used for the analysis of turbulent flow around rotor models. The pressure–velocity coupling is achieved using the well-known SIMPLE method by Patankar [23]. Turbulence kinetic energy (*k*) and turbulence dissipation rate (*ε*) first-order upwind scheme was chosen for the momentum equation solution. The standard *k-ε* turbulence model [24] is a semi-empirical model based on model transport equations for *k* and its *ε*. The model transport equation for *k* was derived from the exact

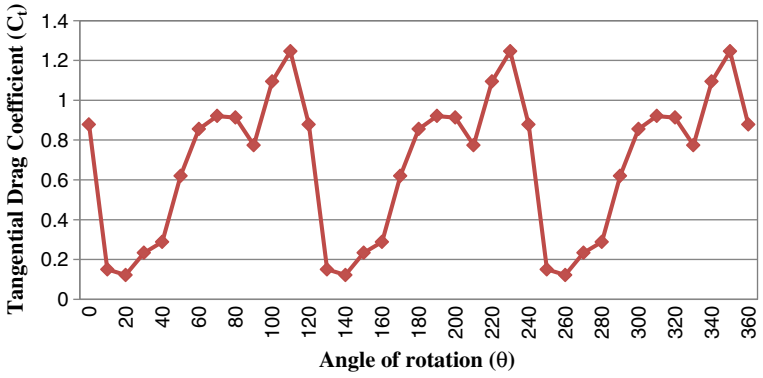

Figure 8 C_t **versus angle of rotation (*θ*) for the three-bladed rotor.**

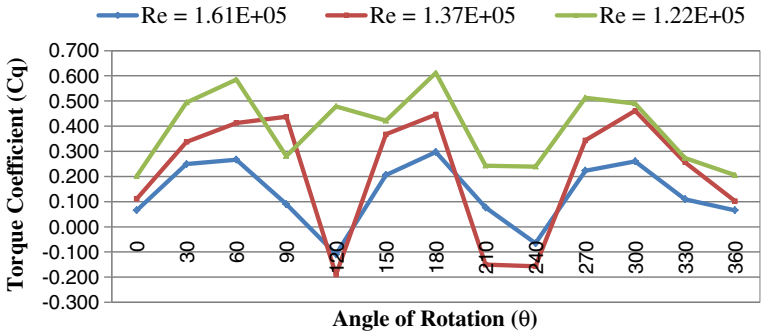

Figure 9 C_q **versus angle of rotation (*θ*) for model 1.**

equation, while the model transport equation for ε was obtained using physical reasoning and bears little resemblance to its mathematically exact counterpart.

The turbulence kinetic energy, k, and its rate of dissipation, ε, were obtained from the following transport equations:

$$\frac{\partial}{\partial t}(\rho k)+\frac{\partial}{\partial x_i}(\rho k u_i)=\frac{\partial}{\partial x_j}\left[\left(\mu+\frac{\mu_t}{\sigma_k}\right)\frac{\partial k}{\partial x_j}\right]+G_k+G_h-\rho\varepsilon-Y_M+S_k, \tag{13}$$

$$\frac{\partial}{\partial t}(\rho \varepsilon)+\frac{\partial}{\partial x_i}(\rho \varepsilon u_i)=\frac{\partial}{\partial x_j}\left[\left(\mu+\frac{\mu_t}{\sigma_\varepsilon}\right)\frac{\partial \varepsilon}{\partial x_j}\right]+c_{1\varepsilon}\frac{\varepsilon}{k}(G_k+C_{3\varepsilon}G_b)-C_{2\varepsilon}\rho\frac{\varepsilon^2}{k}+S_\varepsilon. \tag{14}$$

In these equations, G_k represents the generation of turbulence kinetic energy due to the mean velocity gradients; G_b, the generation of turbulence kinetic energy due to buoyancy; Y_M, the contribution of the fluctuating dilatation in compressible turbulence to the overall dissipation rate; and $C_{1\varepsilon}$, $C_{2\varepsilon}$, and $C_{3\varepsilon}$, constants. σ_k and σ_ε are the turbulent Prandtl numbers for k and ε, respectively. S_k and S_ε are user-defined source terms. The turbulent (or eddy) viscosity, μ_t, is computed by combining k and ε as follows:

$$\mu_t=\rho C_\mu\frac{k^2}{\varepsilon}, \tag{15}$$

where C_μ is a constant.

Boundary conditions were assigned with symmetric top and bottom, the left side was open with inlet free-stream velocity, and the right side was open with an atmospheric pressure outlet. Inlet air velocity was considered the same as the experimental values, i.e., 9.66, 8.23, and 7.33 m/s, and air density was considered at 1.2 kg/m^3. The blades were considered as moving walls and their rotational velocity was provided from the rpm measured during the experiment. The convergence of the sequential iterative solution is achieved when the sum of the absolute differences of the solution variables between two successive iterations falls below a prespecified small number, which was chosen as 1×10^{-5} in

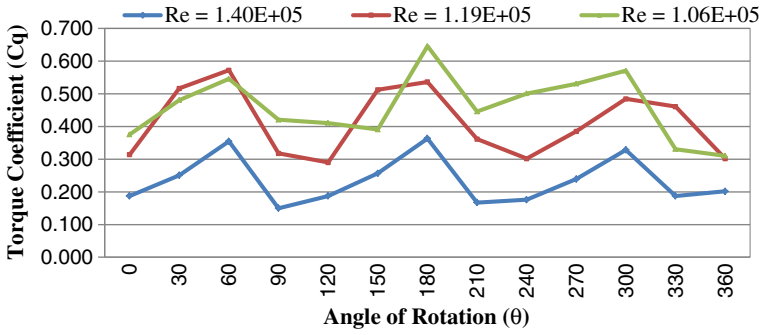

Figure 10 C_q **versus angle of rotation (*θ*) for model 2.**

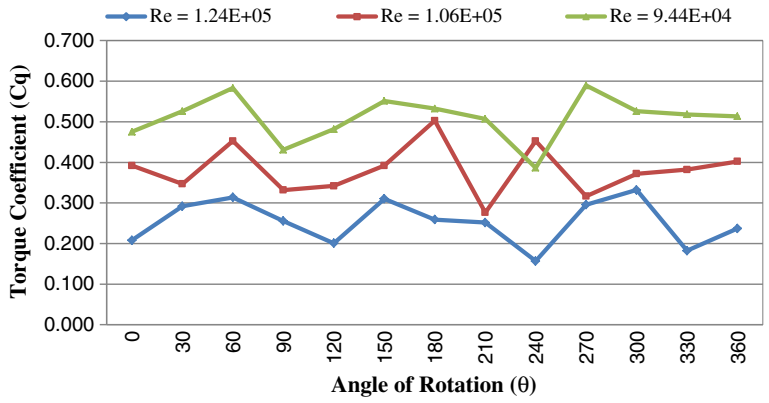

Figure 11 C_q versus angle of rotation (θ) for model 3.

this study. For all models using k-ε turbulence model convergence criteria, 1×10^{-5} was set and tested for continuity, x velocity, y velocity, k, and ε.

Results and discussion

Experimental results

Normal and tangential drag coefficients

Normal drag coefficient (C_n) variation with the change in angle of rotation (θ) for the three-bladed Savonius wind turbine model is shown in Figure 7. A three-blade combined effect at every 10° interval from 0° to 360° is shown in this plot. Normal drag coefficient increases with the increase of rotor angle from 0° to 60° and then decreases with the increase of rotor angle up to 100°. Normal drag coefficient is responsible for torque generation in the rotor model. The same pattern of normal drag coefficient repeats from 120° to 230° and from 240° to 350°.

Tangential drag coefficient (C_t) with change in rotor angle (θ) for every 10° interval from 0° to 360° is shown in Figure 8. The figure shows that a sharp drop occurs from 0° to 10° and then sharp increase occurs from 10° to 40°. Again, a sharp drop occurs in the tangential drag coefficient from 40° to 90°, and a sharp increase occurs from 90° to 120°. However, for every angle of rotation, the tangential drag coefficient remains positive which is a very important factor for producing thrust in the rotor model. The same pattern of tangential drag coefficient repeats from 120° to 230° and from 240° to 350° of angle of rotation.

Torque coefficient variation for three individual Savonius VAWT models

Torque coefficient of the Savonius wind turbine model 1 was calculated for three different Reynolds number. Figure 9 shows torque coefficient (C_q) variation with the increase of angle of rotation (θ). Torque coefficient was calculated for combined blade effect at every 30° interval from 0° to 360°. Three Reynolds numbers for model 1 were 1.61×10^5 (for wind speed 9.66 m/s), 1.37×10^5 (for wind speed 8.23 m/s), and 1.22×10^5 (for wind speed 7.33 m/s). For every Reynolds number, the values of

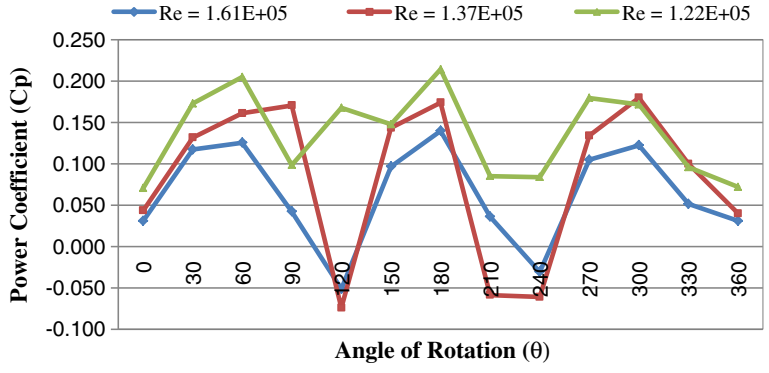

Figure 12 C_p versus angle of rotation (θ) for model 1.

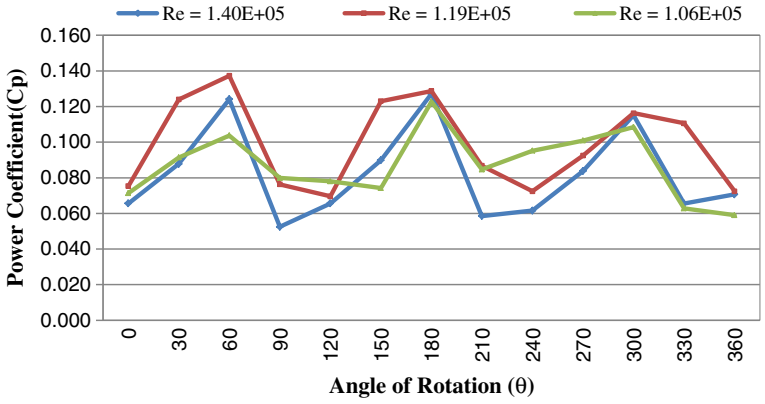

Figure 13 C_p versus angle of rotation (θ) for model 2.

torque coefficient increase from 0° to 60° and then start to decrease from 60° to 120°. The same pattern repeats for the rotor angle from 120° to 210° and from 240° to 330°. For Reynolds number, 1.00×10^5, the value of torque coefficient becomes negative at 120°, 210°, and 240°. It is desired to remove the negative torque for all rotor positions, as this negative torque causes reverse rotation which can reduce power output. Figure 10 shows C_q variation with the angle of rotation (θ) for rotor model 2. Similarly, the combined blade effect on torque coefficient with 30° interval from 0° to 360° was calculated. Reynolds numbers for model 2 were 1.40×10^5 (for wind speed 9.66 m/s), 1.19×10^5 (for wind speed 8.23 m/s), and 1.06×10^5 (for wind speed 7.33 m/s). From the figure, it can be seen that the torque coefficient increases from 0° to 60° and decreases at 90°, and again increases at 120° (except at $Re = 1.06 \times 10^5$). There was no negative torque coefficient for this model. The same pattern repeats for the rotor angle from 120° to 210° and from 240° to 330°. Figure 11 shows C_q variation with the increase of angle of rotation (θ) for model 3. Likewise other two models, combined blade effect on torque coefficient at every 30° interval from 0° to 360° was calculated. Reynolds numbers for model 3 were 1.24×10^5 (for wind speed 9.66 m/s), 1.06×10^5 (for wind speed 8.23 m/s), and 9.44×10^5 (for wind speed 7.33 m/s). For $Re = 1.24 \times 10^5$, 1.06×10^5, and 9.44×10^5, the pattern of the graph looks similar. The torque coefficient increases from 0° to 60° then decreases at 90°, and again increases at 120° (except for $Re = 1.24 \times 10^5$). The same pattern repeats for the rotor angle from 120° to 210° and from 240° to 330°.

Power coefficient variation for three individual Savonius VAWT models

Power coefficient (C_p) was calculated using the relationship between C_p and C_q which is $C_p = C_q \times \lambda$ at three different Re for all three models. Figure 12 shows C_p variation with angle of rotation (θ) from 0° to 360° for model 1. Trends of the plots are similar for $Re = 1.61 \times$

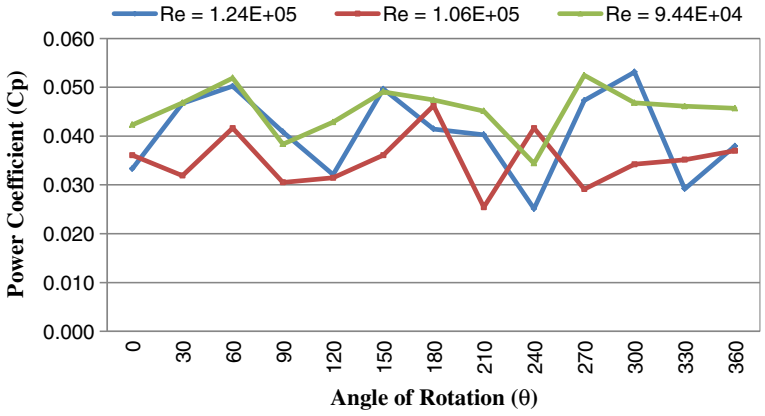

Figure 14 C_p versus angle of rotation (θ) for model 3.

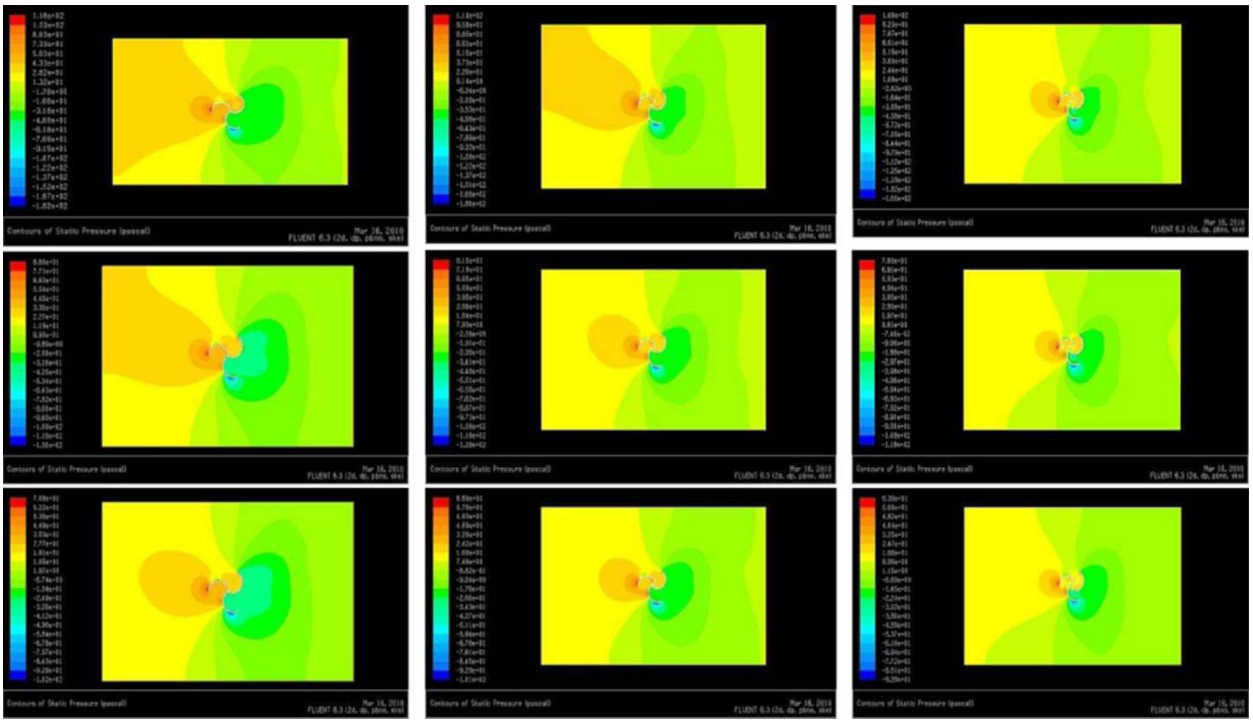

Figure 15 Pressure contours around Savonius rotor (a) model 1, (b) model 2, (c) model 3 for all three Reynolds numbers. (Reynolds numbers in descending order from top to bottom).

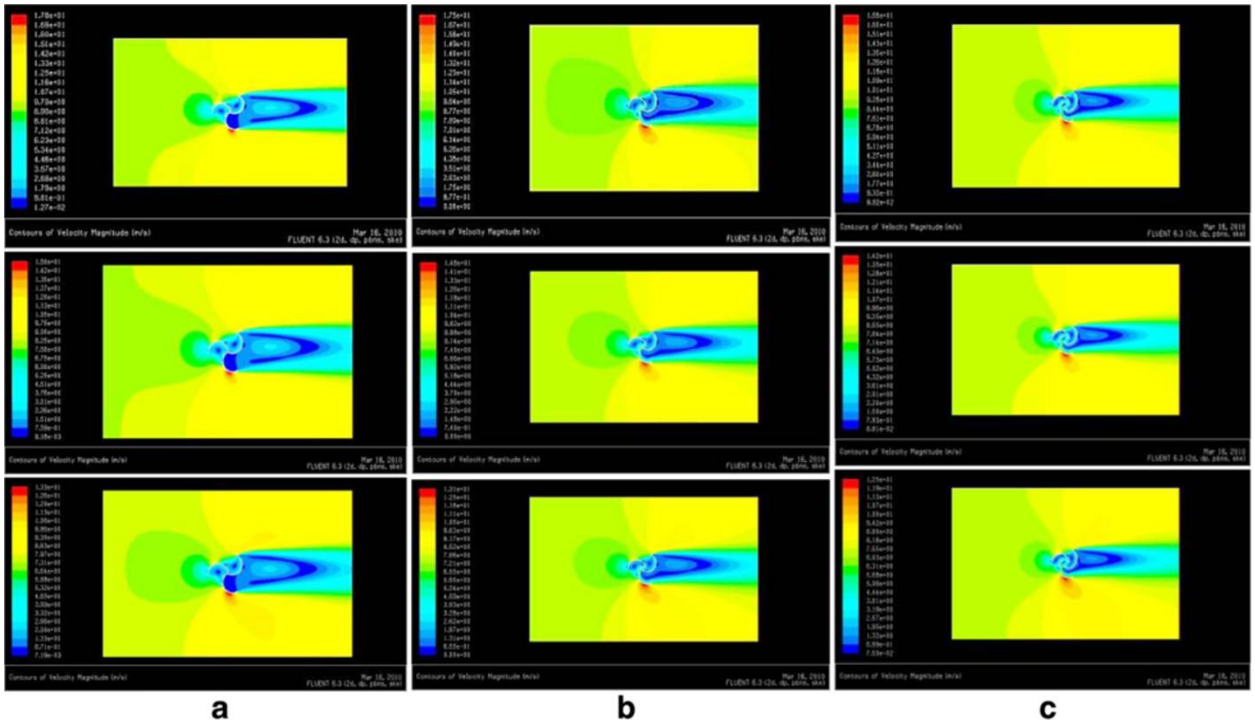

Figure 16 Velocity contours around Savonius rotor (a) model 1, (b) model 2, (c) model 3 for all three Reynolds numbers. (Reynolds numbers are in descending order from top to bottom).

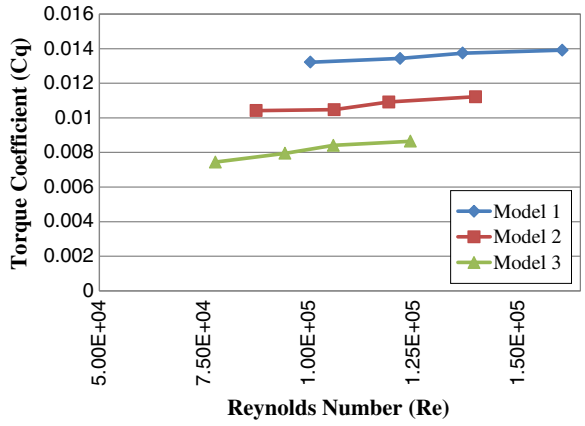

Figure 17 Numerical C_q versus *Re* for three models.

10^5, 1.37×10^5, and 1.22×10^5. Power coefficient was negative at 120°, 210°, and 240° for $Re = 1.37 \times 10^5$ and at 120° and 240° for $Re = 1.61 \times 10^5$. For this model, better power coefficient variation occurred at $Re = 1.22 \times 10^5$. Figure 13 shows C_p variation with angle of rotation (θ) at three different *Re* for model 2. There is no negative power coefficient for this model at any Reynolds number. Figure 14 shows C_p variation with the change of angle of rotation (θ) from 0° to 360° for model 3. For this model, power coefficient variation follows the similar trend for all Reynolds number, increasing from 0° to 60° and then decreasing up to 120° then repeats from 120° to 230° and from 240° to 330°.

Numerical results

Pressure contours for three models at three different Reynolds numbers

Pressure contours generated from numerical simulation of model 1, model 2, and model 3 for three different Reynolds numbers are shown in Figure 15a,b,c, respectively. For all these cases, higher pressure values were found at the convex side of the first blade Savonius rotor model. Negative pressure region was developed from the convex side of blade 2 to some portion of the convex side of blade 3. This negative pressure is creating pressure difference between the concave and convex surfaces that eventually rotates the turbine blades.

Velocity contours for three models at three different Reynolds numbers

Contours of velocity magnitude for Savonius rotor model 1, model 2, and model 3 at three different Reynolds numbers are shown in Figure 16a,b,c, respectively. Patterns of the contours are almost the same for different Reynolds numbers; the only exception is a slight variation in velocity magnitude. Once the wind strikes the turbine blades, the velocity starts to decrease at the trailing edge of the Savonius wind turbine model, but after some distance travel, the turbine blades start to regain their velocity. Higher velocity region was created at the top and bottom sides of the wind turbine model.

Numerical torque coefficient

Figure 17 shows the numerically calculated C_q variation with different *Re* for three different models. With the increase of Reynolds number, the torque coefficient slightly increases for all three models. Model 1 gives better torque coefficient compared to the other two models.

Comparison of numerical and experimental power coefficients

Numerical C_p was calculated by multiplying the numerical C_q and λ. Figures 18, 19 and 20 show the comparison of numerically and experimentally calculated C_p of the three Savonius rotor models with the increase of λ. Converged solutions of the power coefficient values were considered at all tip speed ratios for numerical results, whereas the power coefficient at four rotor positions 0°, 30°, 60°, and 90° were considered for experimental values. Combined blade effect was considered for both experimental and numerical calculations. Figure 18

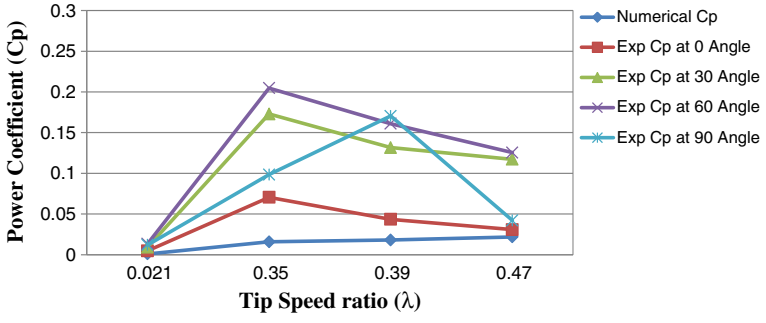

Figure 18 C_p versus λ for model 1.

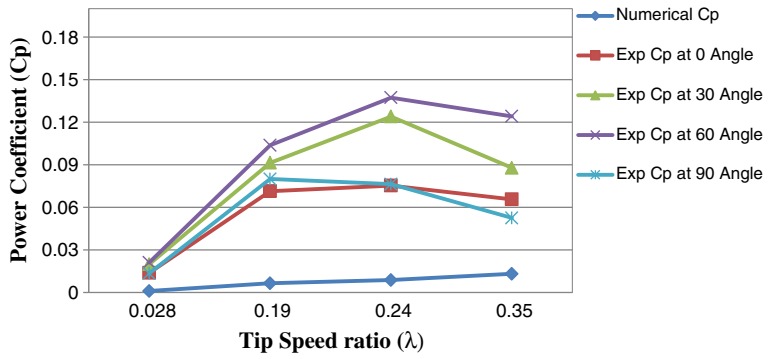

Figure 19 C_p versus λ for model 2.

shows that for model 1 experimental power coefficient at rotor position 0° is very close to the numerical results. However, the deviation is huge for rotor position 60°. Disturbance from the surrounding environment causes a sudden power coefficient increase for the experimental value at different rotor positions, whereas for numerical calculation of power coefficient, the boundary effect has to consider for simulation purpose which causes a reduction in converged numerical power coefficient value. Similar pattern of power coefficient variation is observed for model 2 and model 3 as shown in Figures 19 and 20. However, the magnitude of the C_p decreases for model 2 and model 3 for both numerical and experimental cases.

Error analysis

Normal drag coefficient, tangential drag coefficient, torque coefficient, and power coefficient were calculated both experimentally and numerically and compared. Experimental power coefficient matches well with the numerical results. The experimental results are slightly deviated from the numerical results. In both computational and experimental cases, there can be some possible sources of errors, but computational results are still more towards the ideal case except some assumptions that were made for the model formulation. In the experimental case, more possibilities of errors can be found because of equipment and human imperfection. This could be the reason for lower values of coefficients in the experimental case.

Conclusions

Three different three-bladed Savonius wind turbine scale models with different overlap ratios (model 1, no overlap; model 2, overlap ratio 0.12; and model 3, overlap ratio 0.26) were designed and fabricated for the current study. Aerodynamic characteristics of these models were experimentally investigated using the subsonic wind tunnel. Experimental investigation was performed at different Reynolds numbers. Numerical investigation was also performed to determine torque and power coefficients using GAMBIT and FLUENT. The current study shows that lower Reynolds number gave better C_q variation with the increase of the angle of rotation for each model. Model 2 demonstrates better experimental C_q for all three different wind speeds (9.66, 8.23, and 7.33 m/s). For model 1 with $Re = 1.22 \times 10^5$, model 2 with $Re = 1.19 \times 10^5$, and model 3 with $Re = 9.94 \times 10^4$, the experimental C_p shows higher and positive values compared to other Reynolds numbers. Model 2 shows the better experimental C_p at wind speeds of 9.66 and 8.23 m/s. However, for wind speed 7.33 m/s, model 1 shows the better C_p. Power coefficient calculated from the numerical method shows that it is always increasing with the

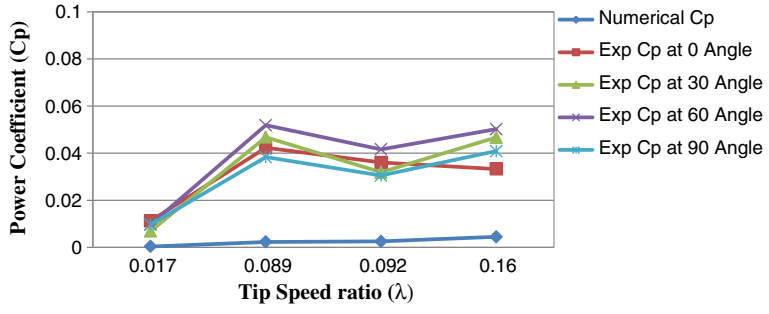

Figure 20 C_p versus λ for model 3.

increase of tip speed ratio. For model 1, numerical power coefficient matches well with the corresponding experimental values at 0° rotor position.

Abbreviations

a: overlap distance between two adjacent blades (mm); *A*: rotor area (m^2); AR: aspect ratio; C_n: normal drag coefficient; C_p: power coefficient; C_q: torque coefficient; C_t: tangential drag coefficient; *d*: blade diameter (mm); *D*: overall rotor diameter (mm); F_n: normal drag force (N); F_t: tangential drag force (N); *H*: rotor height (mm); *k*: turbulence kinetic energy; *N*: rotational speed (rpm); OR: overlap ratio: ratio of overlap distance between two adjacent blades and rotor diameter (OR = *a* / D); *P*: power (W); *Re*: Reynolds number; *T*: torque (N.m); *V*: wind velocity (m/s); *v*: kinematic viscosity (m^2/s); ρ: air density (kg/m^3); θ: angle of rotation (°); Φ: angular position of the pressure tapping points on three blades (°); ω: angular velocity (rad/s); λ: tip speed ratio; Δp: pressure difference (Pa); ε: turbulence dissipation rate.

Competing interests

The authors declare that they have no competing interests.

Authors' contributions

KNM carried out both experimental and computational investigations on the performance improvement of the three-bladed Savonius wind turbine with varying overlap ratios under the supervision of MR. GM and MA were also in the research group who gave their inputs time to time. All authors have their contributions in different percentages in developing the manuscript of this paper. All authors read and approved the final manuscript.

Acknowledgments

The authors acknowledge the funding and facility support from the Mechanical Engineering Department of Georgia Southern University. They would also like to thank Mr. Andrew Michaud for helping in fabricating different Savonius wind turbine models.

Author details

[1]Mechanical Engineering Department, Colorado State University, Fort Collins, CO 80523, USA. [2]Mechanical Engineering Department, Georgia Southern University, Statesboro, GA 30460, USA. [3]Biochemistry, Chemistry & Physics, Southern Arkansas University, Magnolia, AR 71753, USA.

Received: 18 September 2012 Accepted: 8 March 2013
Published: 18 April 2013

References

1. Hayashi, T, Li, Y, Hara, Y, Suzuki, K: Wind tunnel test on a three stage out phase Savonius rotor. JSME International Journal **48**(1), 9–16 (2005)
2. Diaz, F, Gavalda, J, Massons, J: Drag and lift coefficients of the Savonius wind machine. J. Wind. Eng. **1991**(15), 240–246 (1991)
3. Sawada, T, Nahamura, M, Kamada, S: Blade force measurement and flow visualization of Savonius rotors. Bulletin of JSME **29**, 2095–2100 (1986)
4. Aldoss, TK, Obeidat, KM: Performance analysis of two Savonius rotors running side by side using the discrete vortex method. Wind. Eng. **11**, 79–88 (1987)
5. Fujisawa, N, Gotoh, F: Experimental study on the aerodynamic performance of a Savonius rotor. ASME J Sol Energ Eng **116**, 148–152 (1994)
6. Rahman, M, Islam, MQ, Islam, AKMS: Prediction of dynamic characteristics of a three bladed Savonius rotor. In: Proceeding of the third international conference on fluid mechanics and heat transfer. Dhaka, Bangladesh. 15–16 December 1999
7. Rahman, M: Torque and drag characteristics of a three bladed Savonius rotor. Mechanical Engineering Department, Bangladesh University of Engineering and Technology, Bangladesh (1999). M.Sc. thesis
8. Rahman, M, Islam, MQ, Islam, AKMS: Aerodynamic characteristics of a three bladed Savonius rotor. In: Proceeding of the 2nd international seminar on renewable energy for poverty alleviation. IEB, Bangladesh. 26–27 November 1999
9. Rahman, M, Morshed, KN, Lewis, J, Fullar, M: Experimental and numerical investigations on drag and torque characteristics of three-bladed Savonius wind turbine. In: Proceedings of 2009 ASME International Mechanical Engineering Congress and Exposition (IMECE 2009). Lake Buena Vista, Orlando. 13–19 November 2009
10. Gupta, R, Biswas, A, Sharma, KK: Comparative study of a three bucket Savonius rotor with a combined three-bucket Savonius–three-bladed Darrieus rotor. Renew Energy **33**, 1974–1981 (2008)
11. Altan, BD, Atilgan, M, Ozdamar, A: An experimental study on improvement of a Savonius rotor performance with curtaining. Exp. Therm. Fluid. Sci. **32**, 1673–1678 (2008)
12. Sargolzaei, J, Kianifar, A: Modeling and simulation of wind turbine Savonius rotor using artificial neural networks for estimation of the power ratio and torque. Simulat. Model Pract. Theor. **17**, 1290–1298 (2009)
13. Altan, BD, Atilgan, M: An experimental and numerical study on the improvement of the performance of Savonius wind rotor. Energ. Convers. Manag. **49**, 3425–3432 (2008)
14. Saha, UK, Thotla, S, Maity, D: Optimum design configuration of Savonius rotor through wind tunnel experiment. J. Wind. Eng. Ind. Aerod. **96**, 1359–1375 (2008)
15. Kamoji, MA, Kedare, SB: Wind tunnel tests on a single stage helical Savonius rotor. In: 5th AIAA International Energy Conversion Engineering Conference. St. Louis, Missouri. 25–28 June 2007
16. Gupta, R, Das, R, Gautam, R, Deka, SS: CFD analysis of a two bucket Savonius rotor for various overlap conditions. ISESCO J. Sci. Tech. **8**(13), 67–74 (2012)
17. Qasim, AY, Usubamatov, R, Zain, ZM: Investagation and design impeller type vertical axis wind turbine. Australian J Basic Appl Sci **5**(12), 121–126 (2011)
18. Ghatage, SV, Jyeshtharaj, BJ: Optimisation of vertical axis wind turbine: CFD simulations and experimental measurements. Can. J. Chem. Eng. **90**, 1186–1201 (2012)
19. Kumbernuss, J, Chen, J, Yang, HX, Lu, L: Investigation into the relationship of the overlap ratio and shift angle of double stage three bladed vertical axis wind turbine (VAWT). J. Wind Eng. Ind. Aerod. **107**, 57–75 (2012)
20. Carrigan, TJ, Brian, HD, Zhen, XH, Bo, PW: Aerodynamic shape optimization of a vertical-axis wind turbine using differential evolution. International Scholarly Research Network ISRN Renewable Energy **2012**, 1–16 (2012)
21. Morshed, KN: Experimental and numerical investigations on aerodynamic characteristics of Savonius wind turbine with various overlap ratios. Georgia Southern University (2010). M.S. thesis
22. Pinkerton, RB: Calculated and measured pressure distribution over the midspan section of the NACA 4412 airfoil. NACA report no. **563**, 365–380 (1936)
23. Patankar, SV: Numerical Heat Transfer and Fluid Flow. Hemisphere Publishing Corporation, Washington, D.C. (1980)
24. Launder, BE, Spalding, DB: Lectures in Mathematical Models of Turbulence. Academic Press, London (1972)

doi:10.1186/2251-6832-4-18
Cite this article as: Morshed *et al.*: **Wind tunnel testing and numerical simulation on aerodynamic performance of a three-bladed Savonius wind turbine.** *International Journal of Energy and Environmental Engineering* 2013 **4**:18.